Using Image Warping for Time-lapse Image Domain Wavefield Tomography

Di Yang, Alison Malcolm and Mike Fehler, MIT*

Downloaded 07/04/17 to 134.153.188.68. Redistribution subject to SEG license or copyright; see Terms of Use at http://library.seg.org/

SUMMARY

Time-lapse seismic data are widely used for monitoring subsurface changes. A quantitative assessment of how reservoir properties have changed allows for better interpretation of fluid substitution and migration during processes like oil and gas production, and carbon sequestration. Full waveform inversion has been proposed as a way to retrieve quantitative estimates of subsurface properties through seismic waveform fitting. However, for most monitoring systems, the offset range versus depth of interest is not large enough to provide information about the low wavenumber velocity model. In this study, we present a wavefield tomography method using the local warping between baseline and time-lapse images as the cost function. The new cost function is sensitive to volumetric velocity anomalies, and capable of handling large velocity changes, where traditional full waveform inversion fails. In this paper, we first describe the theory and workflow of our method, and then we show a numerical example to demonstrate its advantages.

INTRODUCTION

Time-lapse seismic monitoring is often applied for reservoir management in the oil industry to obtain information about reservoir changes. It helps identify bypassed oil to be targeted for infill drilling which extends the economic life of a field (Lumley, 2001). It is also capable of monitoring the progress of fluid fronts, providing information for injection optimization in enhanced oil recovery and long-term fluid storage like carbon sequestration (Bickle et al., 2007). Generally, one baseline survey and subsequent monitoring surveys are acquired over time. Analysis and comparison of the datasets provides an estimate of changes in seismic velocity and mass density. These changes are related to changes in dynamic reservoir properties like pore pressure and fluid saturation (Dadashpour et al., 2008) that are important in reservoir simulation and interpretation.

To quantitatively recover rock physical parameters, full waveform inversion (FWI) (Tarantola, 1984; Virieux and Operto, 2009) is being tested on individual surveys. The application of FWI to time-lapse data seems straight-forward, however, in practice it is constrained by the survey design, data quality and the nonlinear nature of FWI. Research on inversion strategies tailored for time-lapse data has been proposed regarding the issues like repeatability, computation efficiency (Yang et al., 2012) and local minima (Watanabe et al., 2005; Denli and Huang, 2009; Yang et al., 2011). Traditional FWI requires low frequency data and large survey offsets to invert for the low wavenumber velocity model (Virieux and Operto, 2009). However, seismic surveys with large offsets are expensive and not economical when the region of interest is local and relatively small. In addition, FWI results are more like those of a least-squares migration with small-offset reflection data because the survey does not have enough constraints on the model from different angles to estimate the low-wavenumber structure and so find only the reflectivity. Image domain methods, often involving velocity analysis, have been proposed to obtain the low wavenumber part of the velocity model from reflection data (Sun and Symes, 2012; Biondi and Almomin, 2012). These methods are usually computationally heavier because they require the calculation of angle gathers.

In the time-lapse setting, we assume the subsurface geology structure does not change dramatically over the period of surveys. For example, the physical displacement of the reservoir boundaries caused by compaction may be only a fraction of a sampling interval of the image. Based on this assumption, the successive images of the reservoir should illuminate similar areas at nearly identical locations if correct velocity models are provided.

In this paper, we present an image-domain wavefield tomography (IDWT) method specialized for time-lapse reservoir monitoring. Baseline surface survey data are used in a standard waveform inversion or velocity analysis to obtain a baseline model. Migration images for both baseline and time-lapse data can be produced based on the baseline model. With the assumptions above, the image difference should be primarily caused by changes in the velocity. Dynamic image warping (Hale, 2013) is used to measure the image difference in a way that is robust to cycle skipping. By minimizing the warping function, we invert for the velocity changes iteratively with the adjoint method (Plessix, 2006). In this paper, the theory and workflow of this approach are described. A synthetic example is used to demonstrate its capability.

THEORY

4D image domain wavefield tomography can be considered as the counterpart of full waveform inversion. The cost function here can be written as the L-2 norm of the "distance" between two images. The simplest form is to take the difference between two images:

$$E(m) = \frac{1}{2} \int_x \int_z |I_1(x,z) - I_0(x,z)|^2, \qquad (1)$$

where I_0 is the baseline image and I_1 is the time-lapse image. x and z are spatial coordinates. We derive all the equations here in 2D for simplicity, but the extension to 3D is straightforward. This cost function has the same drawback as the traditional FWI cost function. When the image difference is too large ($>$ half wavelength in the reflector's normal direction), the cycle skipping effect makes the cost function insensitive to local model perturbations. As described by Hale (2013), a migration image based on the incorrect velocity can be considered as a warped version of the true image based on the cor-

© 2013 SEG

DOI http://dx.doi.org/10.1190/segam2013-0662.1

Downloaded 07/04/17 to 134.153.188.68. Redistribution subject to SEG license or copyright; see Terms of Use at http://library.seg.org/

rect velocity. In time-lapse applications, the time-lapse image based on the baseline velocity is a warped version of the baseline image. For images with reflection data, we assume most of the warping is vertical. The amount of vertical warping can be calculated by solving an optimization problem. Specifically we compute

$$w(x,z) = \arg\min_{l(x,z)} D(l(x,z)) \tag{2}$$

where

$$D(l(x,z)) = \int_x \int_z (I_1(x,z) - I_0(x,z+l(x,z)))^2 dxdz \tag{3}$$

We use the dynamic warping algorithm (Hale, 2013) to solve for the warping function $w(x,z)$.

Since the warping function should decrease consistently as I_1 becomes closer to I_0, we use the L-2 norm of $w(x,z)$ as the cost function

$$E(m) = \frac{1}{2}\sum_{x_s}\int_x\int_z |w(x,z,x_s)|^2 dxdz \tag{4}$$

and invert for velocity by minimizing $E(m)$ with a gradient-based method.

To calculate the gradient G, we use an adjoint method. The derivation is similar to the formula in differential semblance optimization (DSO) (Plessix, 2006). The gradient can be written as a correlation between wavefields

$$G = -(< \frac{\partial^2 \lambda_s(t)}{\partial t^2}, u_s(t) > + < \frac{\partial^2 \lambda_r(t)}{\partial t^2}, u_r(t) >) \tag{5}$$

where $u_s(t)$ and $u_r(t)$ are source and receiver fields used for imaging, and $\lambda_s(t)$ and $\lambda_r(t)$ are the associated adjoint wavefields respectively, and $<>$ is the inner product operator in time. The adjoint sources for $\lambda_s(t)$ and $\lambda_r(t)$ are:

$$d_s(x,z,t) = \alpha(x,z) * u_r(t) \tag{6}$$

and

$$d_r(x,z,t) = \alpha(x,z) * u_s(t) \tag{7}$$

in which

$$\alpha(x,z) = \frac{w(z) * \frac{\partial I_0(z+w(z))}{\partial z}}{(\frac{\partial I_0(z+w(z))}{\partial z})^2 - \frac{\partial^2 I_0(z+w(z))}{\partial z^2}(I_1(x,z) - I_0(x,z+w(z)))} \tag{8}$$

A detailed derivation is presented in Yang et al. (2013). The implementation of the inversion process consists of the following steps:

given a baseline velocity model m_0, and a baseline migration image I_0,

(i) for each shot, compute the migration image with time-lapse data based on velocity model m_i

(ii) compute the vertical shifts $w(x,z)$ using dynamic warping

(iii) compute the adjoint wavefields λ_s,λ_r, and gradient G

(iv) update the velocity model with the nonlinear conjugate method using the gradient G^*

(v) remigrate time-lapse data with updated model m_{i+1}, and calculate the cost function $E(m)$

(vi) if $E(m)$ is smaller than a preset value, stop iterating; otherwise, go to step(ii)

SYNTHETIC EXAMPLE

We use a two-layer acoustic model to demonstrate how this approach works. The density model has two discontinuities. The baseline velocity model is constant (v_p=3000m/s). The time-lapse model change is shown in Figure 2. It is a Gaussian-shaped velocity increase, with a maximum value of 800m/s. We place 300 receivers (blue triangles in Figure 1) and 5 sources (red stars in Figure 1) on the surface to generate the datasets.The source is a Ricker wavelet with a center frequency of 25 Hz. In this synthetic example, we assume the baseline model is known. Both conventional FWI and IDWT are applied for the time-lapse data. Their performances are compared to show the advantage of IDWT for model recovery and convergence.

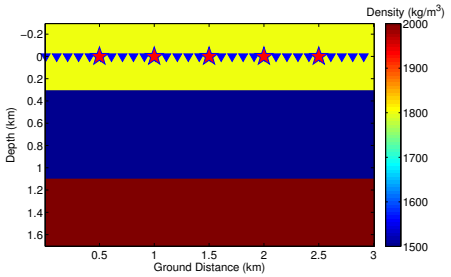

Figure 1: The two-layer density model for both baseline and time-lapse. Red Stars denote the locations of the shots, and blue triangles denote the receiver locations.

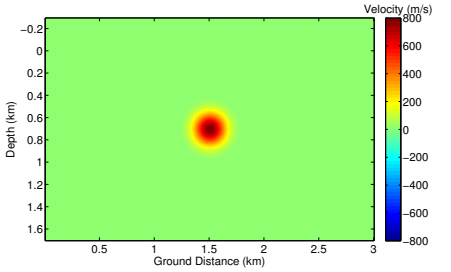

Figure 2: Difference in the P-wave velocities between baseline and time-lapse surveys. Maximum velocity increase is 800m/s.

IMAGING AND WARPING

Reverse time migration (RTM) is utilized to produce all the images during the inversion. The imaging condition is

$$I = \int_{t=0}^{T} < u_s(t), u_r(t) > dt. \tag{9}$$

© 2013 SEG

DOI http://dx.doi.org/10.1190/segam2013-0662.1

The baseline image and initial time-lapse image are shown in Figure 3(a) and Figure 3(b).

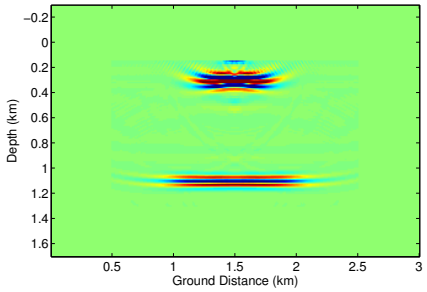

(a)

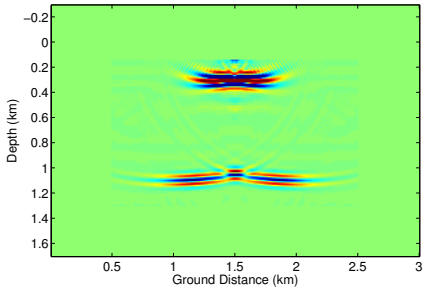

(b)

Figure 3: (a) The baseline image I_0 obtained using one shot gather and the baseline model. (b) The time-lapse image I_1 obtained using one shot gather and the baseline model.

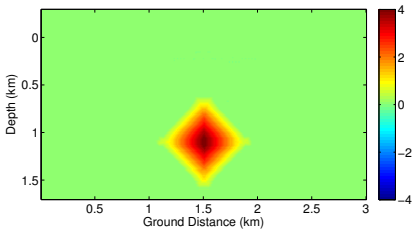

Figure 4: The image warping function $w(x,z)$ calculated from Figure 3(a) and 3(b). Units on the color scale are image points.

The position of the deeper reflector in the time-lapse image (Fig 3(b)) is shifted vertically due to the velocity change in Figure 2. We compute $w(x,z)$ using the dynamic image warping algorithm (Hale, 2013) to describe how much I_1 is shifted from I_0, as shown in Figure 4. The maximum shift is 4 grid points (i.e. 40 meters). As in Equation 8, $w(x,z)$ is used to calculate a spatial weighting function $\alpha(x,z)$, to mask the wavefields u_s and u_r to form adjoint sources (Equation 6 and 7).

INVERSION RESULTS COMPARISON

Figure 5 shows the velocity model change recovered from IDWT. The inverted anomaly is centered at the correct location, but is smeared vertically due to the acquisition geometry. But the vertical smearing is bounded by the reflectors. If any perturbation occurs above the first reflector, the entire image will be shifted. IDWT will correct this shift by reversing that perturbation. Some of the changes are positioned along the ray-path due to limited source/receiver coverage. Within the area of the inverted anomaly, the amplitude is not correctly distributed, and the maximum amplitude of change is only 50% of the true value. We expect this to be improved by adding more shots.

Although the inverted velocity is not perfect, the time-lapse image based on it (Fig 6) is precise enough to put reflectors at the same locations as in the baseline image (Fig 3(a)). The model from IDWT has the correct first-order kinematics, and is a good starting model for FWI. Figure 7 shows the result of a standard FWI based on the model from IDWT. Both the amplitude of the anomaly, and the distribution of the velocity are improved as FWI corrects the higher order kinematics and dynamics.

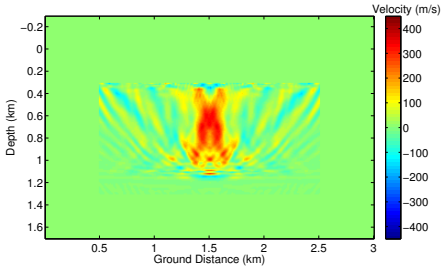

Figure 5: The velocity changes inverted by IDWT.

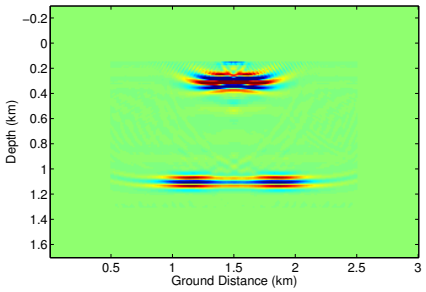

Figure 6: The time-lapse image obtained using one shot gather and the model inverted with IDWT.

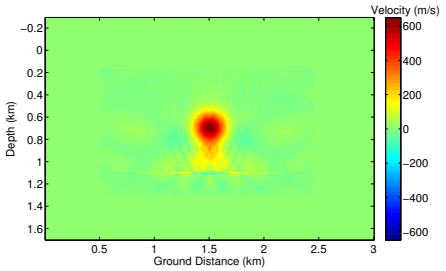

Figure 7: The velocity changes resolved by FWI after IDWT

Downloaded 07/04/17 to 134.153.188.68. Redistribution subject to SEG license or copyright; see Terms of Use at http://library.seg.org/

© 2013 SEG

DOI http://dx.doi.org/10.1190/segam2013-0662.1

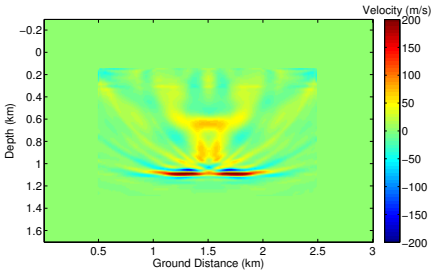

Figure 8: The velocity changes inverted by a standard FWI starting from the baseline model.

A standard FWI is also performed starting from the correct background constant velocity model and the correct density model. Figure 8 shows the final result. The inversion gives poor recovery of the anomaly because of several issues. First, the velocity change is large enough to cause cycle skipping in the data domain. Second, FWI with this narrow-offset survey geometry, reduces to least-squares migration. The volumetric velocity change is barely resolved. Instead, a reflector that does not exist in the true model, is generated to fit the data.

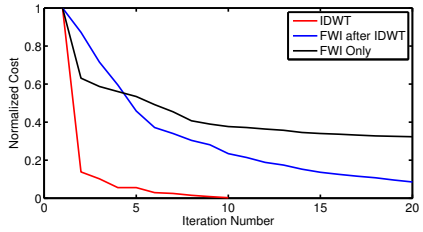

Figure 9: Convergence curves of IDWT (red) and FWI after IDWT (blue).

DISCUSSION

From a computational point of view, the image domain wavefield tomography requires two wavefield extrapolations for each migration. With the same wave equation solver, it takes twice as much time as FWI for each iteration. However, it is not necessary to simulate the full wavefield to form the images. The image warping cost function only requires information about the kinematics, which is robust when the accuracy of the simulated waveform amplitudes are limited. In contrast, traditional FWI needs a high-quality simulation so that the comparison between waveforms is reliable.

Although the apparent calculation time is doubled compared to FWI, IDWT appears to converge very fast (less than 10 iterations). We compare the convergence curves of IDWT, FWI after IDWT and FWI-only in Figure 9. IDWT converges much faster than the FWI based on the IDWT result. Therefore, to resolve the velocity anomaly, the actual computation of IDWT is affordable and does not dominate the cost of the overall process. The FWI-only case plateaued after several iterations. As discussed above, the cycle skipping effect makes the cost function not sensitive to the velocity updates. Ideas similar to image-warping can be implemented in the data domain to avoid cycle-skipping. However, with reflection geometries, FWI fails to invert for volumetric changes in velocity, and the result tends to be like that of a least-squares migration. Ma and Hale (2013) have successfully overcome this problem.

In time-lapse inversions, we are interested in the relative changes between the surveys at different times. However, the residuals due to the uncertainty in the baseline inversion are likely to contaminate the final result. Tailored FWI schemes have been developed to suppress these noises (Denli and Huang, 2009; Yang et al., 2011). In IDWT, the errors in the baseline model are internally taken into account in the baseline migration. As the time-lapse images match the baseline ones, the only perturbation in the velocity model is in the kinematic difference between time-lapse and baseline datasets.

In addition, the signal to noise ratio in migration images is lower than that in data because of stacking. IDWT tries to fit the images where the noise is suppressed. Another concern for time-lapse data, is the repeatability of surveys. In general, the shot and receiver locations are not identical between surveys even for high-quality ocean bottom cables. Moreover, after the initial large survey for exploration, specialized local surveys for monitoring are more economical and efficient. IDWT has no constraints on the survey geometry. As long as the time-lapse data illuminates an area of interest that is also well-imaged with the baseline survey, IDWT can update the local velocity.

As with most tomography methods, IDWT smears the model along ray-paths. More reflectors in the model provide more constraints on the inversion. The vertical resolution of IDWT is at least bounded by the reflector spacing (i.e. the anomaly will not smear across reflectors). For smaller anomalies (e.g., velocity changes caused by overpressure), IDWI can be improved by increasing survey offsets as is the case for most tomography methods. IDWI results can also be used as the starting model for FWI to refine the model or invert for other parameters such as density and S-wave velocity.

CONCLUSIONS

We have proposed a time-lapse wavefield tomography method in the image domain for reflection data. The warping between baseline and time-lapse images is used as a cost function, which is sensitive to smooth velocity perturbations, and robust against cycle-skipping effects. The adjoint method is applied to calculate the gradient and the nonlinear conjugate gradient method is used to update the model iteratively. The method is not limited by discrepancies between survey geometries. The recovery of the volumetric velocity change with IDWT plus FWI is markedly better than with full waveform inversion alone.

ACKNOWLEDGMENTS

This work was supported by the MIT Earth Resources Laboratory Founding Members Consortium.

Downloaded 07/04/17 to 134.153.188.68. Redistribution subject to SEG license or copyright; see Terms of Use at http://library.seg.org/

© 2013 SEG

DOI http://dx.doi.org/10.1190/segam2013-0662.1

http://dx.doi.org/10.1190/segam2013-0662.1

EDITED REFERENCES

Note: This reference list is a copy-edited version of the reference list submitted by the author. Reference lists for the 2013 Annual International Meeting, SEG, Expanded Abstracts have been copy edited so that references provided with the online metadata for each paper will achieve a high degree of linking to cited sources that appear on the Web.

REFERENCES

Bickle, M., A. Chadwick, H. Huppert, M. Hallworth, and S. Lyle, 2007, Modelling carbon dioxide accumulation at Sleipner: Implications for underground carbon storage: Earth and Planetary Science Letters, **255**, 164–176, http://dx.doi.org/10.1016/j.epsl.2006.12.013.

Biondi, B., and A. Almomin, 2012, Tomographic full waveform inversion (TFWI) by combining full waveform inversion with wave-equation migration velocity analysis: 82nd Annual International Meeting, SEG, Expanded Abstracts, http://dx.doi.org/10.1190/segam2012-0275.1.

Dadashpour, M., M. Landrø, and J. Kleppe, 2008, Nonlinear inversion for estimating reservoir parameters from timelapse seismic data: Journal of Geophysics and Engineering, **5**, 54–66, http://dx.doi.org/10.1088/1742-2132/5/1/006.

Denli, H., and L. Huang, 2009, Double-difference elastic waveform tomography in the time domain: 79th Annual International Meeting, SEG, Expanded Abstracts, **28**, 2302–2306, http://dx.doi.org/10.1190/1.3255320.

Hale, D., 2013, Dynamic warping of seismic images: Geophysics, **78**, no. 2, S105–S115, http://dx.doi.org/10.1190/geo2012-0327.1.

Lumley, D. E., 2001, Time-lapse seismic reservoir monitoring: Geophysics, **66**, 50–53, http://dx.doi.org/10.1190/1.1444921.

Ma, Y., and D. Hale, 2013, Personal communication.

Plessix, R.-E., 2006, A review of the adjoint-state method for computing the gradient of a functional with geophysical applications: Geophysical Journal International, **167**, 495–503, http://dx.doi.org/10.1111/j.1365-246X.2006.02978.x.

Sun, D., and W. W. Symes, 2012, Waveform inversion via nonlinear differential semblance optimization: 82nd Annual International Meeting, SEG, Expanded Abstracts, http://dx.doi.org/10.1190/segam2012–1190.1.

Tarantola, A., 1984, Inversion of seismic reflection data in the acoustic approximation: Geophysics, **49**, 1259–1266, http://dx.doi.org/10.1190/1.1441754.

Virieux, J., and S. Operto, 2009, An overview of full-waveform inversion in exploration geophysics: Geophysics, **74**, no. 6, WCC1–WCC26, http://dx.doi.org/10.1190/1.3238367.

Watanabe, T., S. Shimizu, E. Asakawa, and T. Matsuoka, 2005, Differential waveform tomography for time-lapse crosswell seismic data with application to gas hydrate production monitoring: 75th Annual International Meeting, SEG, Expanded Abstracts, http://dx.doi.org/10.1190/1.1845221.

Yang, D., M. Fehler, and A. Malcolm, 2013, Personal communication.

Yang, D., M. Fehler, A. Malcolm, and L. Huang, 2011, Carbon sequestration monitoring with acoustic double-difference waveform inversion: A case study on SACROC walkaway VSP data: 81st Annual International Meeting, SEG, Expanded Abstracts, 4273–4277, http://dx.doi.org/10.1190/1.3628099.

Downloaded 07/04/17 to 134.153.188.68. Redistribution subject to SEG license or copyright; see Terms of Use at http://library.seg.org/

Yang, D., Y. Zheng, M. Fehler, and A. Malcolm, 2012, Target-oriented time-lapse waveform inversion using virtual survey: 82nd Annual International Meeting, SEG, Expanded Abstracts, http://dx.doi.org/10.1190/segam2012-1308.1.

Downloaded 07/04/17 to 134.153.188.68. Redistribution subject to SEG license or copyright; see Terms of Use at http://library.seg.org/